



Effect of Deposition Potential on Synthesis, Structural, Morphological and Photoconductivity Response of Cu₂O Thin Films by Electrodeposition Technique

K. P. Ganesan^{1,2} · N. Anandhan² · T. Marimuthu² · R. Panneerselvam² · A. Amali Roselin²

Received: 2 October 2018 / Revised: 5 December 2018 / Published online: 21 February 2019
© The Chinese Society for Metals (CSM) and Springer-Verlag GmbH Germany, part of Springer Nature 2019

Abstract

The present work describes the effect of deposition potentials on structural, morphological, optical, electrical and photoconductivity responses of cuprous oxide (Cu₂O) thin films deposited on fluorine-doped tin oxide glass substrate by employing electrodeposition technique. X-ray diffraction patterns reveal that the deposited films have a cubic structure grown along the preferential (111) growth orientation and crystallinity of the film deposited at -0.4 V is improved compared to the films deposited at -0.2 , -0.3 and -0.5 V. Scanning electron microscopy displays that surface morphology of Cu₂O film has a well-defined three-sided pyramid-shaped grains which are uniformly distributed over the surface of the substrates and are significantly changed as a function of deposition potential. Raman and photoluminescence spectra manifest that the film deposited at -0.4 V has a good crystal quality with higher acceptor concentration compared to other films. UV–visible analysis illustrates that the absorption of Cu₂O thin film deposited at -0.4 V is notably higher compared to other films and the band gap of Cu₂O thin films decreases from 2.1 to 2.04 eV with an increase in deposition potential from -0.2 to -0.5 V. The frequency–temperature dependence of impedance analysis shows that the film deposited at -0.4 V has a high conductivity. I – V measurements elucidate that the film deposited at -0.4 V exhibits a good photoconductivity response compared to films deposited in other deposition potentials.

Keywords Electrodeposition · Cu₂O thin films · Photoconductivity response · I – V measurement

1 Introduction

In recent years, fabrication of cuprous oxide (Cu₂O) thin films has drawn great interest due to their excellent p -type semiconducting properties such as a direct energy band gap of 2.2 eV with a higher absorption coefficient in visible region around 650 nm [1, 2]. It has a higher hole mobility of $21 \text{ cm V}^{-1} \text{ s}^{-1}$ with large minority carrier diffusion length [2]. The improvement in physical properties of Cu₂O thin films is widely used in various applications such as transistors [3], solar cells [4], nonlinear optical devices

[5], photocatalysis [6], biosensors [7] and magnetic storage devices [8]. Various kinds of physical and chemical deposition methods have been applied to prepare the Cu₂O thin films including radio frequency (RF) magnetron sputtering [9], spray pyrolysis [10], sol–gel [11], pulsed laser deposition [12], chemical vapour deposition [13], thermal oxidation [14] and electrodeposition [15]. Among the various deposition techniques, the use of physical deposition techniques requires higher cost instrument and higher processing temperature with high vacuum chamber to prepare higher quality Cu₂O thin films, whereas electrodeposition is one of the simplest techniques in chemical deposition due to low cost instrument, low processing temperature (< 100) and easy instrument handling compared to other deposition techniques [16, 17]. Generally, the crystal structure, surface morphology and thickness of the films can be easy tailored by adjusting electrodeposition parameters such as solution concentration, solution pH, bath temperature, deposition time and deposition potential [18]. Jiang et al. [19] reported the surface morphology of Cu₂O films which

Available online at <http://link.springer.com/journal/40195>

✉ N. Anandhan
anandhan_kn@rediffmail.com

¹ Department of Physics, Saiva Bhanu Kshatriya College, Aruppukottai 626101, India

² Advanced Materials and Thin Film Laboratory, Department of Physics, Alagappa University, Karaikudi 630003, India

convert octahedral into cubic with an increase in deposition potentials towards more negatives from -0.1 to -0.9 V. Laidou et al. [20] studied the effect of deposition potential on Cu_2O thin films and observed significant changes in morphology and crystallite size as a function of deposition potential. Haller et al. [21] found that Cu_2O film deposited at an optimum deposition potential of -0.9 V showed better crystal quality compared to other deposition potentials. Han et al. [22] reported that the conductivity type of Cu_2O thin film could be changed from *n*-type to *p*-type by controlling the deposition potential from 0 to -0.3 V. Zhao et al. [23] have investigated the effect of deposition potential on Cu_2O films for solar cell applications and observed that the film deposited at -0.7 V exhibited a photoresponse. Mohra et al. [24] found that Cu_2O thin films deposited at various deposition potentials from -0.4 to 0.7 V showed effective modification on structural, optical and electrochemical studies. Jiang et al. [25] reported that when Cu_2O thin films were deposited at various deposition potentials from -0.1 to -0.8 V, the band gap of the films significantly varied in the range from 2.35 to 1.63 eV. From the above literature reviews, most of the researches have focused on the effect of deposition potentials on crystal quality, surface morphology, electrochemical study, band gap and optical properties of the Cu_2O thin films. However, ac electrical conductivity and photoconductivity response of Cu_2O thin film deposited at different deposition potentials have rarely been reported.

In the present work, an attempt has been made to achieve a high crystalline Cu_2O thin film on fluorine-doped tin oxide (FTO) substrate with good ac conductivity and photoconductivity response by employing a lower temperature electrodeposition technique at different deposition potentials from -0.2 to -0.5 V in less-concentration alkaline solution containing 0.15 mol L^{-1} copper sulphate and 1 mol L^{-1} lactic acid. The effect of different deposition potentials (-0.2 to -0.5 V) on structural, morphological, vibrational, optical and electrical properties of electrodeposited Cu_2O thin films was investigated with the help of X-ray diffraction (XRD), scanning electron microscopy (SEM), Raman spectroscopy, photoluminescence spectroscopy, UV-Vis-NIR spectroscopy, LCR metre and Keithley instrument.

2 Experimental

The polycrystalline Cu_2O thin films were electrodeposited on FTO glass substrate by using conventional three-electrode cell system. Prior to electrodeposition of Cu_2O , the FTO substrates were ultrasonically cleaned in acetone, isopropanol and deionized water for 10 min each. Electrochemical cell consisting of FTO substrate, platinum and Ag/AgCl electrodes was used as a working electrode, a counter electrode and a reference electrode, respectively.

The deposition solution contained 0.15 mol L^{-1} copper sulphate pentahydrate ($\text{CuSO}_4 \cdot 5\text{H}_2\text{O}$), 1 mol L^{-1} lactic acid, whose pH was adjusted around 11 by drop wise addition of sodium hydroxide (NaOH) solution. The Cu_2O film was electrodeposited at different deposition potentials (-0.2 to -0.5 V) versus Ag/AgCl at 55°C bath temperature for 30 min by using potentiostat (Model 362, EC & G Princeton Applied Research, USA Instrument). The deposited Cu_2O films were subsequently rinsed in deionized water and were dried at 100°C for 5 min.

An X-ray diffractometer (X'PERT PRO analytic X-ray diffractometer) with $\text{CuK}\alpha$ radiation ($\lambda = 0.15406 \text{ nm}$) was used to study the crystal structure and crystallinity of Cu_2O film. Surface morphological analysis was carried out by using a scanning electron microscope ZEISS instrument. The vibrational properties of the Cu_2O thin films were studied by employing micro-Raman spectroscopy under an excitation wavelength of 515.5 nm using Argon green laser. Photoluminescence spectroscopy (RF-6000, SHIMADZU instrument) was carried out to investigate the luminescence properties of Cu_2O thin films. Optical absorption and transmittance of the deposited Cu_2O films were recorded by using a UV-Vis-IR spectrometer (UV-1800, SHIMADZU instrument). Thickness of the Cu_2O thin films was measured by using a stylus profilometer. Electrical properties of the thin films were studied by using LCR spectroscopy. Photoconductivity (I - V) of the Cu_2O films was carried out by using Keithley semiconductor characterization system 4200 instrument under 100-mW light illumination using Xenon lamp.

3 Results and Discussion

3.1 Structural Analysis

The crystal structure and the crystalline nature of the electrodeposited Cu_2O films were investigated by XRD analysis. Figure 1 shows the XRD patterns of Cu_2O thin films deposited at different deposition potentials of -0.2 , -0.3 , -0.4 and -0.5 V. XRD patterns reveal that the deposited Cu_2O films are polycrystalline in nature and belong to cubic structure. Apart from the diffraction peaks corresponding to the FTO glass substrate, they are indicated by a star symbol and their peaks are at 2θ values of 29.01° , 36.52° , 42.11° and 61.11° corresponding to (110), (111), (200) and (220) diffraction planes, respectively. It shows that they are in good agreement with international centre for diffraction data (ICDD) card No. 75-1531. When the film is deposited at -0.2 V, the intensity of (200) peak is higher compared to the (110), (111) and (220) planes and it indicates the preferential growth of Cu_2O . When there is an increase in the deposition potential from -0.3 to -0.5 V, XRD patterns show a higher intense (111) peak which reveal that the deposition potential

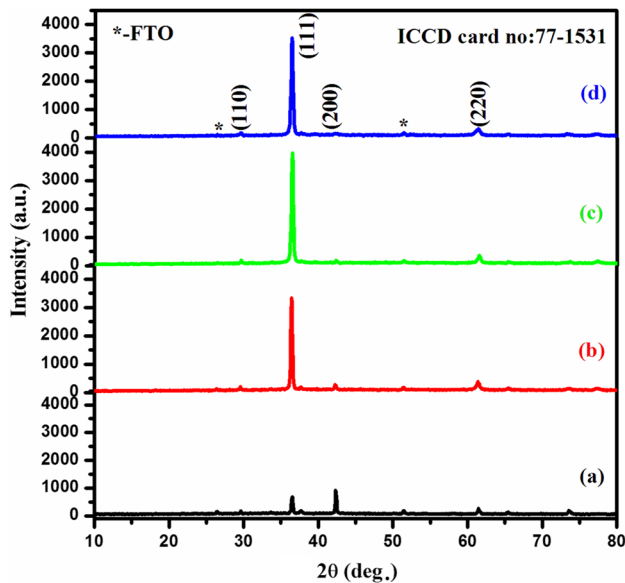


Fig. 1 X-ray diffraction patterns of Cu_2O thin films deposited at different deposition potentials: **a** -0.2 V, **b** -0.3 V, **c** -0.4 V, **d** -0.5 V

obviously changes the crystal growth orientation from (200) to (111) plane. The decrease in (111) peak intensity of the Cu_2O deposited at -0.5 V may act faster in the growth of Cu_2O crystal [26]. Among the Cu_2O thin films deposited at different deposition potentials, the film deposited at -0.4 V shows a stronger (111) diffraction peak and it can be attributed to higher crystalline nature of the film.

The crystallite size of the films deposited at different deposition potentials was estimated by using Scherrer formula (Eq. 1) and is summarized in Table 1 [27].

$$D = \frac{0.9\lambda}{\beta \cos \theta}, \quad (1)$$

where D is the crystallite size, λ is the wavelength of the X-ray, β is the full width at half maximum (FWHM) of the diffraction peak in radians and θ is the diffraction angle. It is observed that when deposition potential increases from -0.2 to -0.3 V, the crystallite size decreases from 44.11 to 31.76 nm and it may be due to the change in crystal growth orientation from (200) to (111) plane. Whenever there is a further increase in deposition potential to -0.4 V, the crystallite size continuously increases to around 35 nm due to

the increase in crystal growth of the film along the (111) plane. There is a slight decrement in crystallite size around 28.37 nm when the film deposits at -0.5 V, and the resultant decrease in crystallite size is due to the faster growth of Cu_2O crystal when deposition potential becomes more negative [28].

The micro-strain (ϵ) of the electrodeposited Cu_2O films was calculated from the FWHM by using the following Eq. (2) [29, 30].

$$\epsilon = \frac{\beta}{4 \tan \theta}, \quad (2)$$

where β is FWHM of the diffraction peaks and θ is Bragg's angle. The dislocation density (δ) is defined as the length of dislocation lines per unit volume of the crystal and is calculated by using the following Eq. (3) [31].

$$\delta = \frac{1}{D^2}. \quad (3)$$

Micro-strain (ϵ) and dislocation density (δ) of Cu_2O thin films electrodeposited at different deposition potentials are given in Table 1. It is observed that the δ and ϵ increase with an increase in deposition potential from -0.2 to -0.3 V. This is due to an increase in defect levels and grain boundaries as well as a decrease in crystallite size [32]. Both ϵ and δ slightly decrease, as the deposition potential increases to -0.4 V. The decrease in ϵ and δ indicates the presence of a lower number of lattice imperfections and formation of higher quality films. There is a further increase in deposition potential to -0.5 V. Both δ and ϵ increase due to lattice imperfections and defects.

The stacking fault probability (α) is estimated from the formula (4) [33],

$$\alpha = \left[\frac{2\pi^2}{45\sqrt{3}} \right] \left[\frac{\Delta 2\theta}{\tan \theta} \right]. \quad (4)$$

Stacking fault probability of the Cu_2O thin film mainly depends on peak shift of the predominant diffraction peaks with respect to ideal positions of the diffraction peaks. The stacking fault probability and film thickness of films deposited at different deposition potentials are given in Table 1. The stacking fault probability of Cu_2O films continuously

Table 1 Microstructural parameters of the Cu_2O thin films

Potential (V)	Crystallite size, D (nm)	Dislocation density, $\delta \times 10^{14}$ (lines m^{-2})	Micro-strain, ϵ ($\times 10^{-3}$ lines $^{-2}$ m^{-4})	Stacking fault probability, α
-0.2	44.11	5.13	0.754	6.86
-0.3	31.76	9.91	0.792	3.80
-0.4	35.00	8.16	0.669	1.50
-0.5	28.37	12.42	0.720	0.60

decreases with an increase in deposition potential from -0.2 to -0.5 V. The film thickness is dependent on solution concentration, deposition potential and bath temperature. The film thickness gradually decreases from 2.20 to 1.38 μm , as the deposition potential increases from -0.2 to -0.5 V. It is attributed to an increase in the compactness of the films [34].

3.2 Surface Morphological Analysis

SEM images of Cu_2O thin films deposited at different deposition potentials of -0.2 , -0.3 , -0.4 and -0.5 V are shown in Fig. 2. The Cu_2O thin film deposited at a constant deposition potential of -0.2 V displays that a three-sided pyramid-shaped grains are uniformly distributed over the surface of the substrate as shown in Fig. 2a, b. The average grain size of the three-sided pyramid is found to be around 1.06 μm . Moreover, an increase in the deposition potential to around -0.3 V will not result in any morphological changes generated in three-sided pyramid-shaped grains as shown in Fig. 2c, d, but its size notably decreases and is found to be around 0.86 μm . Whenever there is an increase in deposition potential to -0.4 V, the size of the three-sided pyramid-shaped grains further decreases to around 0.6 μm as shown in Fig. 2e, f. It can be observed from Fig. 2a–f that when the deposition potentials increase from -0.2 V to -0.4 V, the sizes of the three-sided pyramid grains continuously decrease without any morphological changes, whereas the number of three-sided pyramid grains obviously increases due to an increase in nucleation of Cu_2O crystal as the deposition potential becomes more negative. Further, the deposition potential increases to -0.5 V as the morphology of the film drastically changes from three-sided pyramid into irregular grains as shown in Fig. 2g, h. The average size of the grains is approximately 0.5 μm . The three-sided pyramid surface morphology of the electrochemically Cu_2O thin films deposited by using electro-deposition technique has also been shown in the previous report [35]. In the present work, it is observed that the film deposited at -0.4 V shows a dense three-sided pyramid-shaped grains leading to multiple reflection of an incident photon. Hence, the film deposited at -0.4 V is more suitable for solar cell applications [35].

3.3 Raman Spectrum Analysis

In order to study the vibrational modes and their crystalline nature, the Raman spectra of the Cu_2O thin films deposited at different deposited potentials of 0.2 , -0.3 , -0.4 and -0.5 V were recorded in the wavelength range from 100 to 800 cm^{-1} (Fig. 3). Three Raman characteristic peaks appear at around 212 , 428 and 630 cm^{-1} , and they confirm regarding the formation of Cu_2O . The high intense peak

which appears at 210 cm^{-1} is assigned to second-order overtone mode $2\Gamma_{15}$ cm^{-1} as well as Raman-allowed mode of the Cu_2O films [36, 37]. The weak peak at 428 cm^{-1} can be ascribed to four phonon mode $3\Gamma_{12} + \Gamma_{25}^+$. The Raman peak at 630 cm^{-1} is attributed to the infrared-allowed mode [38]. It can be confirmed from Raman spectra that the strongest peak of 212 cm^{-1} of the film deposited at -0.4 V shows a good crystalline nature in comparison with films deposited in other deposition potentials. The obtained results are found to be in good agreement with XRD results.

3.4 Photoluminescence (PL) Spectrum Analysis

Photoluminescence (PL) spectra for films deposited at different deposition potentials were carried out to investigate the atomic defects and their crystal quality under an excitation wavelength of 470 nm (Fig. 4). Two emission peaks appear at 590 and 700 nm. The PL peak is observed at 590 nm (2.1 eV) and is assigned to the nearest band edge emission due to electron hole recombination shown in inset of Fig. 4. The intensity of the peak continuously increases as the deposition potentials increases up to -0.4 V and then decreases, which reveals that the film deposited at -0.4 V possesses higher crystal quality compared to other films [39]. The obtainable band edge emission energy gap is well evident with UV–Vis band gap [40]. The PL peak which appears at 700 nm (1.7 eV) is due to Cu vacancy (or) oxygen interstitial. The intensity of the peak increases with deposition potential up to -0.4 V and then decreases. It indicates that the film deposited at -0.4 V shows more Cu vacancy. From the study, it is observed that the films deposited at -0.4 V show more copper vacancy with good crystal quality and is in good agreement with XRD results.

3.5 UV–Visible Spectrum Analysis

The optical absorption spectra were recorded to determine the absorption coefficient and electron transition in Cu_2O semiconducting thin films [18]. UV–visible absorption spectra of Cu_2O thin films deposited at different deposition potentials in the wavelength range of 450 – 900 nm are shown in Fig. 5. Generally, the absorbance depends on the crystal structure, morphology, surface roughness and film thickness [11]. It can be observed from Fig. 5 that Cu_2O thin films deposited at different deposition potentials have band edge absorption peak in visible region due to electron transition from valence band to conduction band. The Cu_2O film deposited at -0.4 V shows a higher optical absorbance than films deposited in other deposited potentials due to the availability of higher density of three-sided pyramid-shaped granular grain in thin film leading to multi-scattering of the

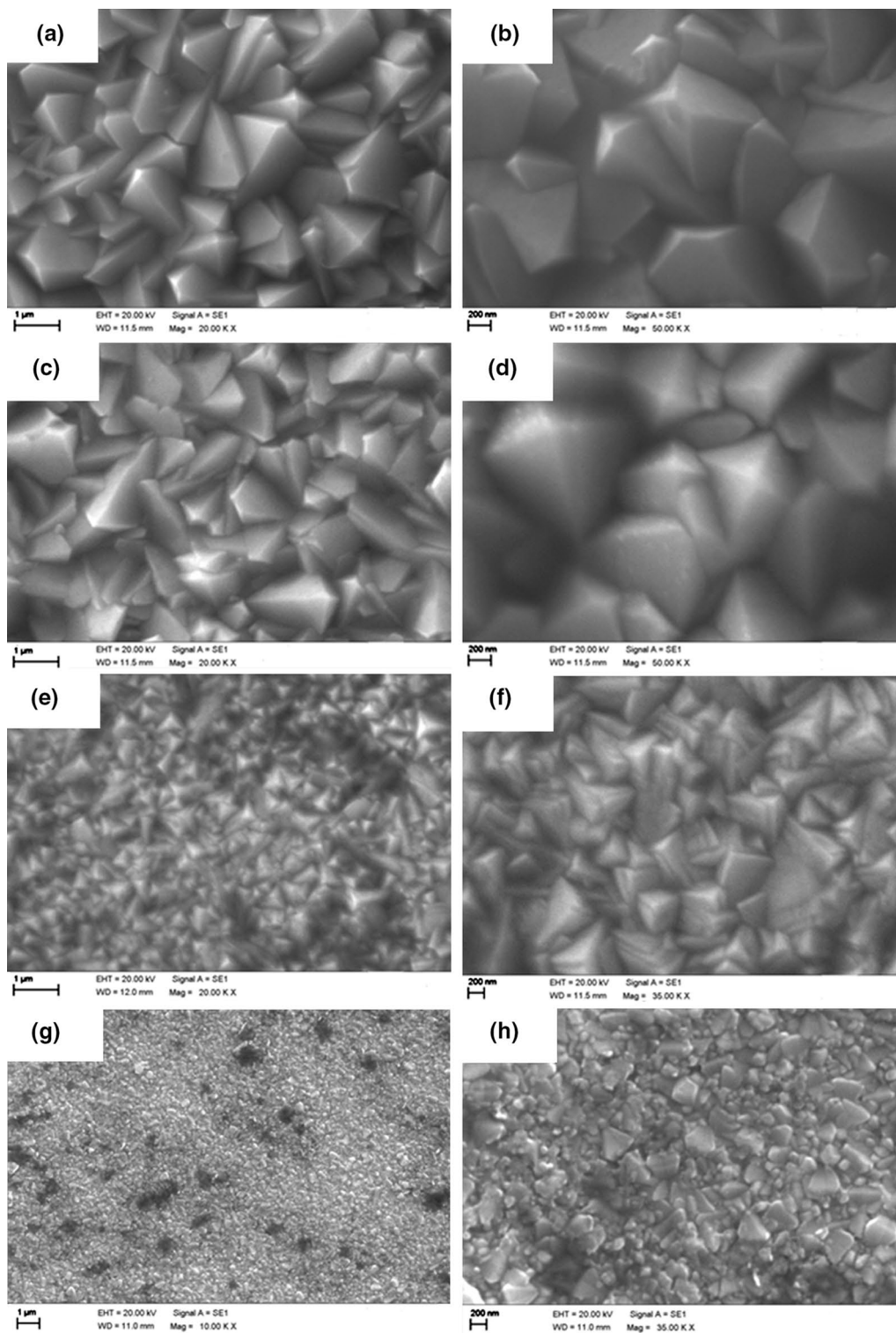


Fig. 2 SEM micrograph of Cu_2O thin films deposited at different deposition potentials: **a, b** -0.2 V , **c, d** -0.3 V , **e, f** -0.4 V , **g, h** -0.5 V

incident light at grain boundaries for absorbing more number of photons. It is observed that the absorbance edge of the film is slightly red, and it shifts from 614 to 644 nm

with an increase in deposition potential. The shifting (red shift) towards higher wavelength is attributed to distortion of $\text{O}-\text{Cu}-\text{O}$ bond in Cu_2O thin films [41]. The optical

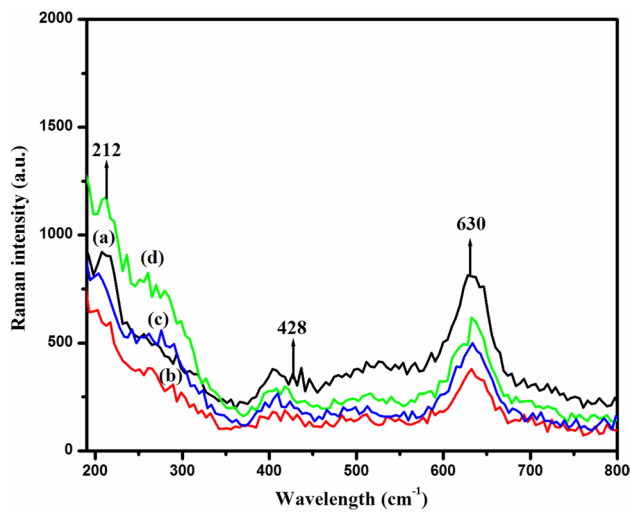


Fig. 3 Raman spectra of Cu_2O thin films deposited at different deposition potentials: **a** -0.2 V, **b** -0.3 V, **c** -0.4 V, **d** -0.5 V

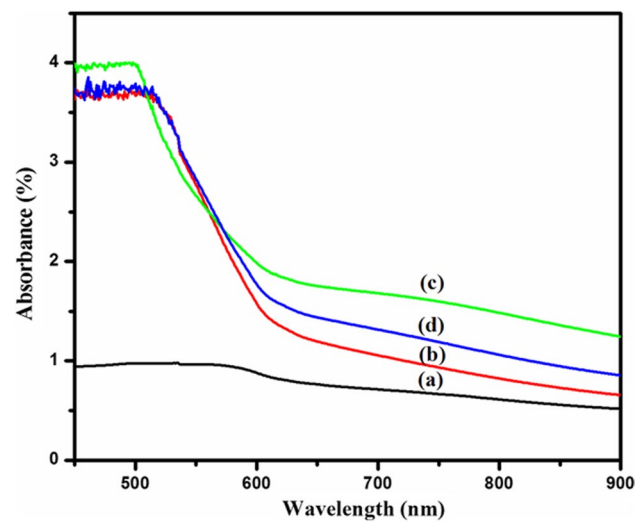


Fig. 5 Absorption spectra of Cu_2O thin films deposited at different deposition potentials: **a** -0.2 V, **b** -0.3 V, **c** -0.4 V, **d** -0.5 V

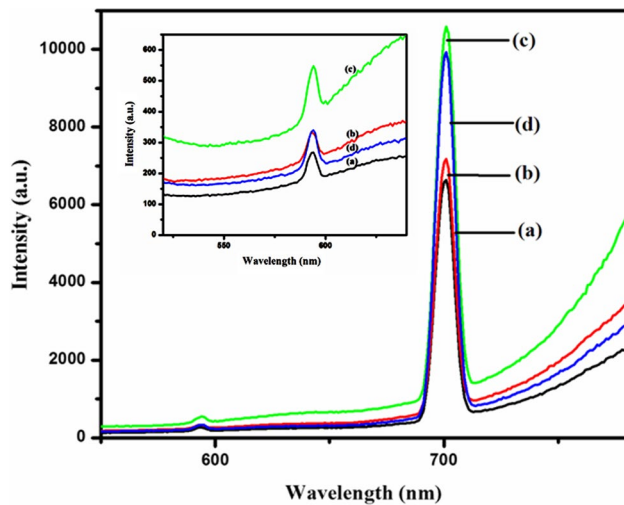


Fig. 4 PL spectra of Cu_2O thin films deposited at different deposition potentials: **a** -0.2 V, **b** -0.3 V, **c** -0.4 V, **d** -0.5 V

absorption and the transmittance are used to investigate the optical parameters such as absorbance coefficient, nature electron transition and optical band gap (E_g) of Cu_2O thin films. The absorption coefficient satisfies Eq. 5 for a direct band gap material [42].

$$\alpha = \frac{1}{t} \ln \left(\frac{A}{T} \right), \quad (5)$$

where α is the absorption coefficient, A is the optical absorbance, T is the transmittance and t is the thickness of the thin films.

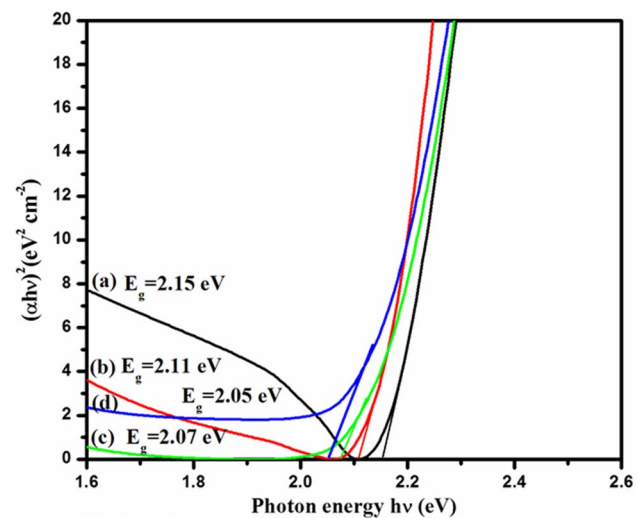


Fig. 6 Tauc's plots of Cu_2O thin films deposited at different deposition potential: **a** -0.2 V, **b** -0.3 V, **c** -0.4 V, **d** -0.5 V

The band gap of Cu_2O thin films is calculated by using Tauc's plot [42].

$$(\alpha h\nu)^2 = A(h\nu - E_g), \quad (6)$$

where α is the absorption coefficient, A is the constant and $h\nu$ is the discrete photon energy. In order to find out the optical band gap, the plot of $(\alpha h\nu)^2$ versus $h\nu$ was drawn as shown in Fig. 6. The energy band gap (E_g) is obtained by extrapolation of linear line intercepting on x -axis. The estimated band gap of the Cu_2O films is 2.15, 2.11, 2.07

and 2.05 eV for films deposited at -0.2 , -0.3 , -0.4 and -0.5 V, respectively. The values of optical band gap of Cu_2O thin films deposited by electrodeposition are similar to the previous reports [20, 23]. The decrease in band gap of the Cu_2O films can be attributed to an improvement in the crystallinity, morphological changes of the films and structural defects in the films [43].

3.6 Electrical Analysis

The ac electrical conductivity can be calculated by using the dielectric data obtained from LCR measurement, and their relation is given below [44].

$$\sigma_{ac} = \omega \epsilon_r \epsilon_0 \tan \delta, \quad (7)$$

where ω is the angular frequency, ϵ_r is the relative permittivity, ϵ_0 is the permittivity of free space and $\tan \delta$ is the loss tangent which is defined as $\tan \delta = \epsilon''/\epsilon'$ where ϵ'' and ϵ' are imaginary and real parts of relative permittivity, respectively. The real part of the relative permittivity is given by Eq. (8) [45].

$$\epsilon' = \frac{Cd}{\epsilon_0 A}, \quad (8)$$

where C is the capacitance of the films, d is the thickness of the films, A is the area of the films and ϵ_0 is the permittivity of the free space ($\epsilon = 8.85 \times 10^{-12}$ F m $^{-1}$). The variations of ac electrical conductivity as a function of frequency at different sample temperatures for Cu_2O thin films deposited at different deposition potentials of 0.2 , -0.3 , -0.4 and -0.5 V are shown in Fig. 7. It is observed from Fig. 7 that the ac conductivity of Cu_2O thin films deposited at different deposition potentials increases with an increase in sample temperatures due to negative temperature coefficient of the impedance [46]. Figure 7 reveals that the ac conductivity of the Cu_2O thin films increases with an increase in deposition potentials. The increment in conductivity of the Cu_2O thin films may be due to the decrease in resistivity and increase in hole density which conform to an acceptor level (copper vacancy). The obtained results are in good agreement with PL result. Hence, Cu_2O thin films deposited at -0.4 V show higher ac electrical conductivity than films deposited in other deposition potentials of -0.2 , -0.3 and -0.5 V.

3.7 I - V Characterization Analysis

The photoconductivity response of Cu_2O thin films deposited at different deposition potentials was carried out under

dark and illumination conditions. The electrical contacts of the deposited film were created on the thin film with 0.5-cm spacing by using silver paste and then connected to Keithley 4200 semiconductor characterization system. Later on, the film is illuminated with an Xenon flash lamp (100 mW). The dark and the photocurrent were measured by applying the input potential in the range from -2 to 2 V. I - V curves of the films deposited at different deposition potentials are shown in Fig. 8. The observed linear I - V curves of the Cu_2O thin film reveal the ohmic nature of the contact. From these curves, it is observed that the Cu_2O thin film deposited at deposition potential -0.4 V exhibits a good photoconductivity response compared to Cu_2O thin films deposited at other deposition potentials. This increased photoconductivity response under illumination may be due to an increase in the conductivity of film which is in inverse proposition to resistivity [47]. Hence, the Cu_2O thin films deposited at deposition potential -0.4 V are more adaptable for solar cell fabrication.

4 Conclusions

Three-sided pyramid-shaped Cu_2O thin films were deposited on FTO glass substrate in different deposition potentials at constant deposition temperature of 55 °C by applying electrodeposition technique. The effect of deposition potentials on structural, morphological, vibrational, optical, electrical and photoconductivity properties was investigated with the help of XRD, SEM, Raman, UV-Vis, LCR and Keithley instrument, respectively. The XRD patterns revealed that the deposited films were found to be in cubic structure and the film deposited at -0.4 V showed good crystalline in nature and was grown along with (111) plane. The SEM images displayed dense and uniform distributed three-sided pyramid-shaped grains for a film deposited at a deposition potential of -0.4 V. The optical properties revealed that a direct band gap value of Cu_2O thin films was estimated to be between 2.0 and 2.1 eV. Micro-Raman and PL spectra revealed that Cu_2O film deposited at deposition potential of -0.4 V showed a good crystal quality at more acceptor level compared to films deposited in other deposition potentials. I - V and LCR measurements showed Cu_2O thin films deposited at deposition potential of -0.4 V, and they had the highest photo- and ac conductivity. From this work, it is evident that the film deposited at -0.4 V is the more suitable material for solar cell applications.

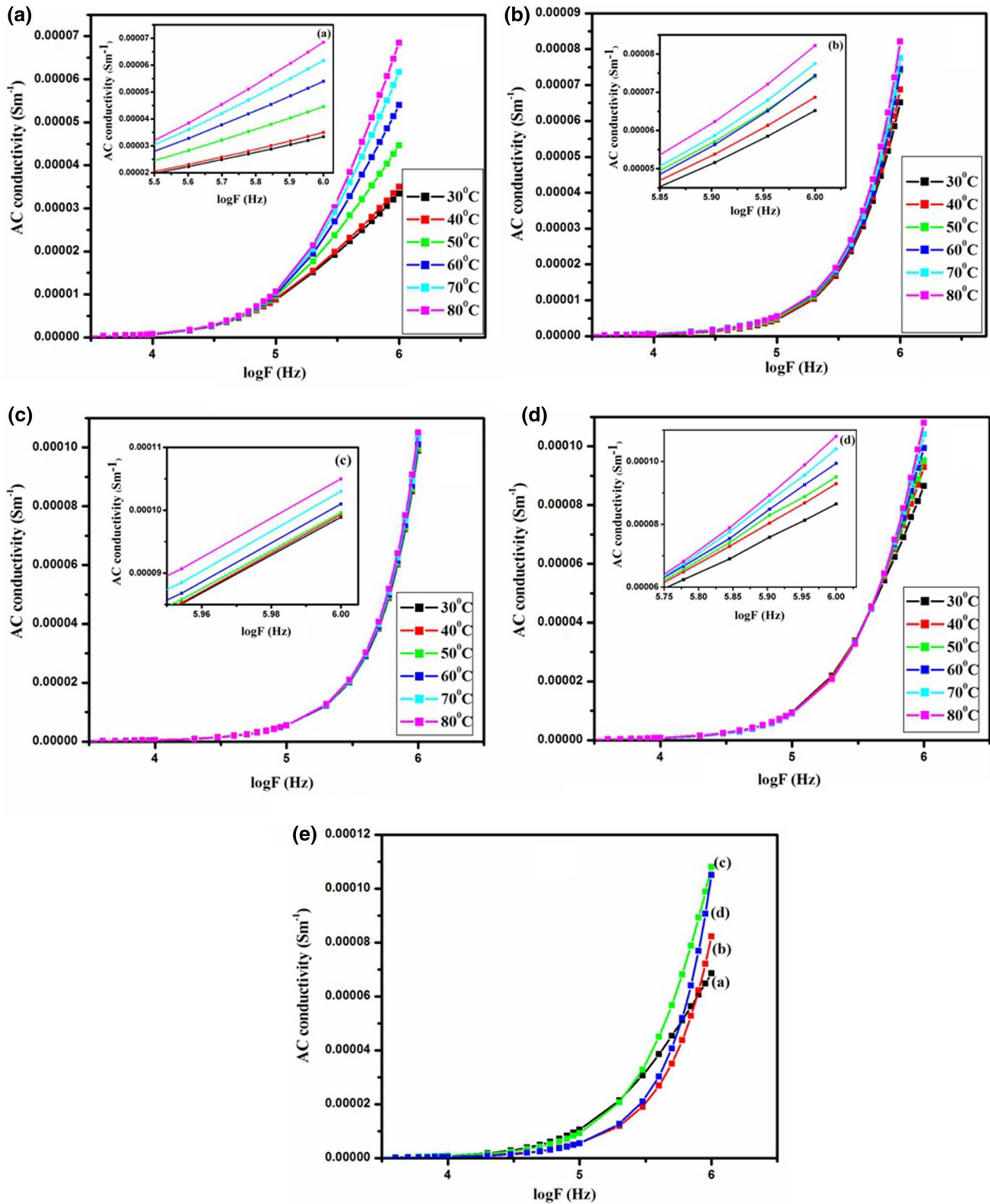


Fig. 7 Temperature-dependent ac electrical conductivity of Cu_2O thin films deposited at different deposited potentials: **a** -0.2 V, **b** -0.3 V, **c** -0.4 V, **d** -0.5 V, **e** ac electrical conductivity carried out at 80°C

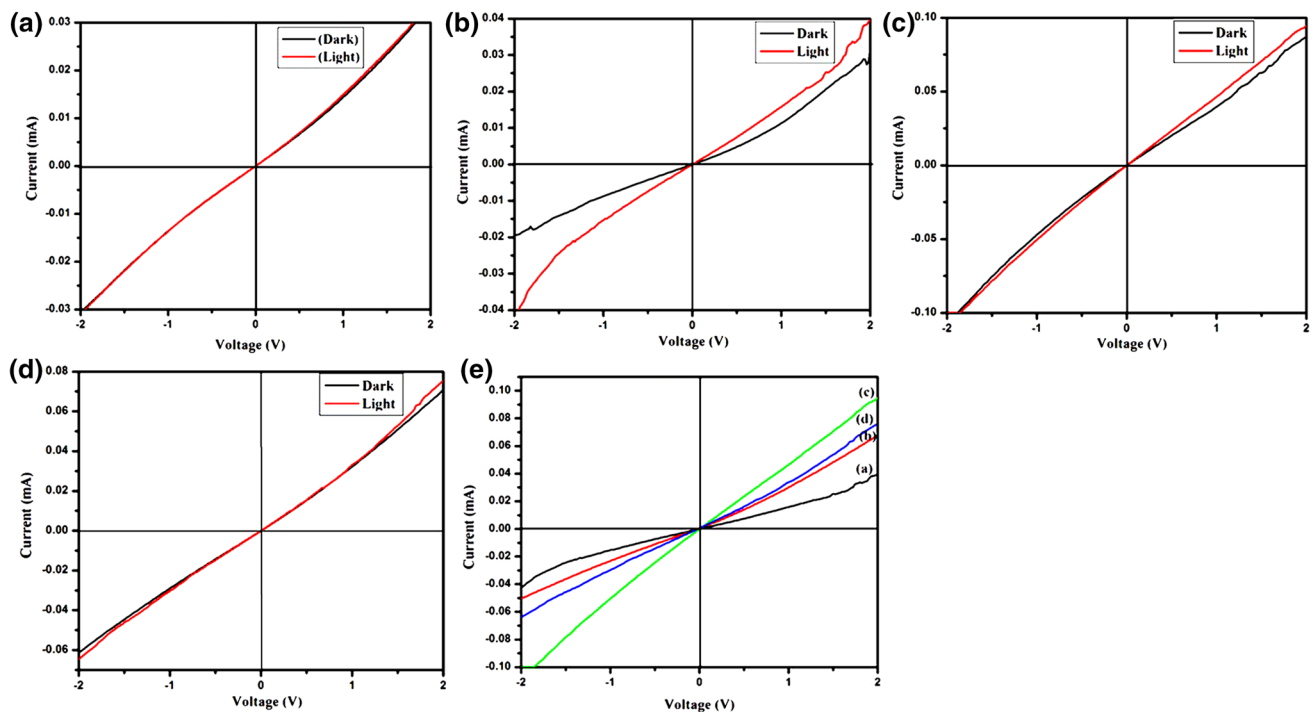


Fig. 8 I - V characteristic curves recorded under the dark and illumination conditions for Cu_2O thin films deposited at different deposition potentials: **a** -0.2 V, **b** -0.3 V, **c** -0.4 V, **d** -0.5 V and **e** I - V characteristic curves under light luminescence

Acknowledgements We gratefully acknowledge the funding and support from the RUSA-Phase 2.0 grant sanctioned vide Letter. No. F. 24-51/2014-U, Policy (TNMulti-Gen), Dept. of Edn. Govt. of India. Dt. 09.10.2018.

References

- [1] G.P. Pollack, D. Trivich, *J. Appl. Phys.* **46**, 163 (1975)
- [2] M. Izaki, S. Sasaki, F. Binti Mohamed, T. Shinagawa, *Thin Solid Films* **520**, 1779 (2011)
- [3] R.G. Delatorre, M.L. Munford, R. Zandonay, V.C. Zolden, *Appl. Phys. Lett.* **88**, 233504 (2006)
- [4] A. Mittiga, E. Salza, F. Sarto, M. Tucci, R. Vasanthi, *Appl. Phys. Lett.* **88**, 163502 (2006)
- [5] G. Yang, A. Chen, M. Fu, H. Long, P. Lu, *J. Appl. Phys. A* **104**, 171 (2010)
- [6] S. Song, R. RaO, H. Yang, A. Zhang, *J. Phys. Chem. C* **114**, 13998 (2010)
- [7] C. Wang, B. Geng, J. Liu, Y. Zhao, *Cryst. Eng. Commun.* **13**, 697 (2011)
- [8] A. Ahmed, N.S. Gaibhiyle, S. Kurian, *J. Solid State Chem.* **183**, 2248 (2010)
- [9] V.F. Drobny, D.L. Pulfrey, *Thin Solid Films* **61**, 89 (1979)
- [10] D. Osorio-Rivera, G. Torred-Delgado, J. Marquez-Marin, *J. Mater. Sci.: Mater. Electron.* **29**, 851 (2018)
- [11] D.S.C. Halin, I.A. Talib, A.R. Daud, *Int. J. Photoenergy* **2014**, 1 (2014)
- [12] A. Chen, H. Long, X. Li, Y. Li, G. Yang, P. Lu, *Vacuum* **83**, 927 (2009)
- [13] G.F. Pan, S.B. Fan, J. Liang, Y.X. Liu, *RSC Adv.* **5**, 42477 (2015)
- [14] M.J. Chen, C.Y. Wu, Y.M. Kuo, *J. Appl. Phys. A* **108**, 133 (2012)
- [15] K.P. Ganesan, N. Anandhan, V. Dharuman, P. Sami, R. Panneerselvam, T. Marimuthu, *Results Phys.* **7**, 82 (2017)
- [16] T. Marimuthu, N. Anandhan, R. Thangamuthu, S. Surya, *J. Mater. Sci.: Mater. Electron.* **29**, 12830 (2018)
- [17] T. Marimuthu, N. Anandhan, R. Thangamuthu, *J. Mater. Sci.* **53**, 12441 (2018)
- [18] T. Marimuthu, N. Anandhan, R. Thangamuthu, *Appl. Surf. Sci.* **428**, 385 (2018)
- [19] X. Jiang, M. Zhan, S. Shi, G. He, X. Song, Z. Sun, *Nanoscale Res. Lett.* **9**, 219 (2014)
- [20] S. Laioudi, A.Y. Bioud, A. Azizi, G. Schmerber, *Semicond. Sci. Technol.* **28**, 15005 (2013)
- [21] S. Haller, J. Jung, J. Rousset, D. Lincot, *Electrochim. Acta* **82**, 402 (2012)
- [22] J. Han, J. Chang, R. Wei, *Int. J. Hydrogen Energy* **43**, 13764 (2018)
- [23] M. Zhao, Y. Jiang, J. Lv, *J. Mater. Sci.: Mater. Electron.* **27**, 1799 (2016)
- [24] D. Mohra, M. Benhaliliba, M. Serin, *J. Semicond.* **37**, 103001 (2016)
- [25] X. Jiang, M. Zhang, S. Shi, *J. Electrochem. Soc.* **161**, D640 (2014)
- [26] D. Yan, S. Li, M. Hu, S. Liu, Y. Zhu, M. CaO, *Sens. Actuators B:Chem.* **211**, 318 (2015)
- [27] T. Marimuthu, N. Anandhan, R. Thangamuthu, M. Mummoothi, S. Rajendran, G. Ravi, *Mater. Res. Express* **2**, 015502 (2016)
- [28] L. Wan, *AIP Conf Proc.* **1995**, 020017 (2018)

- [29] H.P. Klug, L.E. Alexander, X-ray Diffr. *Proced. Polycryst. Amorph. Mater* **992**, 1 (1974)
- [30] T. Mahalingam, V. Dhanasekaran, K. Sundraram, A. Kathalingam, J.K. Rhee, *J. Ionics* **18**, 299 (2012)
- [31] T. Marimuthu, N. Anandhan, R. Thangamuthu, S. Surya, *Superlattices Microstruct.* **98**, 332 (2016)
- [32] S.B. Qadri, E.F. Skelton, D. Hsu, A.D. Dinsmore, J. Yang, H.F. Gray, B.R. Rata, *Phys. Rev. B* **60**, 9191 (1999)
- [33] M. Abdelfatah, J. Ledig, *J. Electrochem. Soc.* **5**, 183 (2016)
- [34] S. Chatterjee, S.K. Saha, A.J. Pal, *Sol. Energy Mater. Sol. Cells* **147**, 17 (2016)
- [35] W. Septina, S. Ikeda, M. Alam Khan, *Electrochim. Acta* **56**, 4882 (2011)
- [36] S. Wu, Z. Yin, Q. He, G. Lu, X. Zhou, H. Zhang, *J. Mater. Chem.* **21**, 3467 (2011)
- [37] S. Eisemann, A. Kronenberger, A. Laufer, J. Bieber, G. Hass, S. Lautenschlager, G. Homm, P.J. Klar, B.K. Meyer, *Phys. Stat. Solid A* **209**, 513 (2012)
- [38] M. Abdelfatah, J. Ledig, A. El-Share, A. Sharafeev, *J. Solid State. Sci. Technol.* **5**, Q183 (2016)
- [39] M.C. Huang, T. Hai Wang, W.S. Chang, J.C. Lin, C.C. Wu, *Appl. Surf. Sci.* **301**, 369 (2014)
- [40] Y. Liu, C. Liu, R. Mu, H. Yang, C. Shao, J.Y. Zhang, Y.M. Lu, D. Shen, X.W. Fan, *Semicond. Sci. Technol.* **20**, 44 (2005)
- [41] Z. Min, L.V. Yao, J. Guo, S. Yue, C. Li, H. Gang, *J. Mater. Sci. Mater. Electron.* **25**, 1799 (2015)
- [42] T. Marimuthu, N. Anandhan, R. Thangamuthu, M. Mummoorthi, G. Ravi, *J. Alloys Compd.* **677**, 211 (2016)
- [43] Y. Akaltun, M. Aliyildirim, A. Stes, M. Yidirim, *Optics Commun.* **284**, 2307 (2011)
- [44] T. Acharya, R.N.P. Chouhary, *Mater. Chem. Phys.* **177**, 131 (2016)
- [45] I. Latif, T.B. Alwan, A.H. Al-Dujaili, *Nanosci. Nanotechnol.* **2**, 190 (2012)
- [46] A. Rawat, H.K. Mahavar, A. Tanwar, *Bull. Mater. Sci.* **37**, 273 (2014)
- [47] T. Logu, R. Raliya, K. Sethuraman, *Cryst. Eng. Commun.* **1039**, 1 (2017)